Microsc. Microanal. Microstruct. **4** (1993) 539–560 DECEMBER **1993**, PAGE 539

Classification
Physics Abstracts
07.80

Quantitative microanalysis using electron energy-loss spectrometry. I. Li and Be in oxides

Ferdinand Hofer and Gerald Kothleitner

Forschungsinstitut für Elektronenmikroskopie, Graz University of Technology, Graz, A-8010, Austria

(Received December 09, 1993; accepted December 23, 1993)

Abstract. — Electron energy-loss spectrometry enables the detection of Li and Be via the K ionization edges. However, the detection and quantification of these low energy edges present several problems, like low edge-to-background ratios, problems with background extrapolations, overlapping of edges and multiple scattering in case of thicker specimens. All these problems can be overcome by careful application of well known procedures: Spectra have to be recorded from very thin specimen regions ($t/\lambda < 0.5$) and subsequently deconvoluted by the Fourier-log-method. This procedure improves the background in front of the edges, so that the conventional $A \cdot E^{-r}$ model can be used for background fitting without problems. The Li and Be K edges overlap with other edges e.g. the L_{23} edges of elements Mg to P and the M_{23} edges of the elements Ca to Cu. In such a situation quantitative analysis is only possible by a multiple-least-square fit with reference spectra and if experimentally determined partial cross-sections are used. The successful application of these methods is demonstrated for inorganic materials like phenacite, beryl, spodumene, Be-phosphate and Li-Cr-oxide. The quantification and detection limits for Li and Be in typical material science specimens are discussed.

1. Introduction.

Within the last few years, electron energy-loss spectrometry (EELS) in an analytical electron microscope (AEM) has found numerous applications in the materials and biological sciences [1]. EELS enables the compositional analysis of chemical elements on a submicrometre scale and is currently the only electron microscopical technique to detect Li and Be which can be analyzed by means of the K ionization edges lying in the low loss region near the plasmon peak and hence exhibiting a low peak-to-background ratio. The Li K edge is found at 55 eV and the Be K edge at 111eV. Attempts have been also made to use X-ray spectrometry in the AEM for the detection of these elements, but both energy-dispersive and wavelength dispersive spectrometry have been of limited used due to the inherent physical limitations of these methods [2]. The K-shell X-rays of Li and Be have low energies and extremely low fluorescence yields. Therefore solid state X-ray detectors (Si(Li) and Ge) are currently incapable of analyzing Li and only particular detectors in

the scanning electron microscope enable the detection of Be in pure Be metal [3]. Other analytical techniques such as Auger spectroscopy and secondary ion mass spectrometry are very sensitive to the presence of Li and Be, however, they lack the spatial resolution of EELS, being less than some nm.

Despite the great importance of Li and Be in materials science, EELS has been only scarcely used for the analysis of these light elements, as shown in the investigations of Liu and Williams on Li-Al alloys [4,5] and Ti-Be intermetallic phases [6]. Liu and Williams demonstrated that quantitative analysis of Li and Be is principally possible but very difficult. Even with these simple compounds data have to be carefully processed using measurements on internal standards.

Although EELS quantification procedures have been established some years ago [7], EELS is mostly used as a qualitative tool. This is due to several problems that remain in the process of extracting absolute or relative concentrations of a given atomic species from the raw spectral data. The limits originate from several sources:

1.1 SPECIMEN THICKNESS. — EELS analysis tends to be very dependent upon specimen thickness. Spectra should be taken only from very thin specimen regions, being thinner than the half of the mean free path of inelastic scattering ($t/\lambda < 0.5$). Otherwise spectra have to be deconvoluted in order to remove multiple scattering contribution.

1.2 INTENSITY DETERMINATION. — The continuously decreasing background must be subtracted from the signal of interest for each element. Although the high-energy tail generally approximates to a power-law energy dependence ($A \cdot E^{-r}$), problems can arise in case of low energy edges. So alternative background subtractions have been proposed particularly for the K edges of Li and Be [8-10]. Another problem arises from closely spaced edges: Li and Be K edges are overlapping with the M_{23} edges of the first row transition metals and with the L_{23} edges of Mg, Al and Si. The separation of the edges is a particular problem and limitation to accurate quantification.

1.3 IONIZATION CROSS-SECTIONS. — In order to convert the edge intensities into elemental concentrations it is necessary to know the ionization cross-section for the relevant ionization edges either absolutely or relatively to those of the other elements present. The ionization cross-sections can be either calculated using Hartree-Slater methods [11, 12] or hydrogenic models [13, 14], or by measuring from standard samples like binary oxides [15, 16]. Although the knowledge on ionization cross-sections has been enormously increased during the last five years, there are still some uncertainties especially in the low energy-loss region. Therefore we will discuss this quantification step thoroughly.

All these problems are essentially enhanced in case of the quantification of Li and Be in minerals and technical materials as it will be demonstrated below. However, these difficulties can be overcome by careful spectrum acquisition and data processing.

In this paper, we present some practical examples for EELS-quantification which is in continuous development in our laboratory. We will describe the quantitative analysis of Li and Be in silicate minerals and oxide materials. All these compounds cannot be quantified using thin-film EDX-spectrometry in the AEM. The present study intends to explore the possibilities of EELS for detection of Li and Be and to provide a guide for quantitative microanalysis of such low energy-loss edges. In a following paper we will present examples for quantification of heavy elements.

2. Experimental procedures.

All samples were prepared for EELS analysis by crushing selected crystals in alcohol and pipetting the suspension onto holey carbon grids. Some minerals were also prepared by ion-milling: In this case single crystals were cut into discs of 3 mm diameter with an ultrasonic drill, dimpled to about 20 μm, then ion-milled with Argon ions at 5 KeV, 0.7 mA and an incidence angle of 12°. Thin film standards were prepared by evaporation of Be, Al, Si and LiF on NaCl crystals. Using a quartz thickness monitor, film thicknesses were measured to be about 15 nm. The thin films were floated off in water and the metals were subsequently oxidized by heating in air at selected temperatures to obtain the desired oxide compounds. EELS experiments were performed in a Philips CM20 Transmission Electron Microscope (TEM) fitted with a Gatan 607 electron spectrometer in sequential acquisition mode. Spectra were collected at 200 kV primary energy, with a beam convergence (α) of 1.5 mrad and an acceptance angle (β) of 7.6 mrad . This acceptance angle has been found to be optimal, because the edge-to-background ratio in the low-loss region depends on this acceptance angle - it is higher for small acceptance angles. On the other hand the acceptance angle β should not be too small, because this may introduce systematical errors in deconvolution procedures. The analyses were performed in TEM image mode (i.e. diffraction coupling) with a screen magnification in the range 5000 to 30000. The energy resolution in the spectra defined by the *FWHM* of the zero loss peak was measured to be between 2 and 2.5 eV. Since the spectra were sampled with a dispersion of 0.5 eV per channel and with 1024 channels per readout, we had to record two spectra which were scaled together afterwards: Beginning with the low loss region and the low energy edges, we subsequently recorded the higher energy edges (e.g. O K and F K edges).

Owing to the very high dynamic range (10^6-10^7) of the spectra, when both the low-loss region and the ionization-edges are to be recorded, special attention to the correct recording conditions has to be given: We acquired the low-loss region in the analog (voltage-to-frequency) mode up to an energy loss of 30 to 50 eV, after which a switchover was made to pulse counting. A gain change of typically 1000x to 3000x resulted from the switchover. Special care was taken to avoid saturation effects when recording the Li and Be K edges with pulse counting, i.e. less than 1×10^5 counts per channel (dwell time 100 ms) were acquired [17].

The Li compounds had to be investigated with a liquid-nitrogen-cooled specimen holder to minimize mass loss of Li.

3. Data analysis.

First, the dark current from the analog part of the spectrum was subtracted. Secondly, the gain change which was set between plasmon peak and the ionization edges was removed by extrapolating both parts of the divided spectrum fitting a third-order polynomial and finally scaling up the low-loss part until the two parts matched up smoothly.

3.1 SPECIMEN THICKNESS. — Detection sensitivity and quantification validity of EEL spectra in thicker samples are limited severely by multiple scattering. Therefore spectra were generally taken at the thinnest edges of the crushed crystals. Specimen thickness t was determined from the energy-loss spectra with the plasmon intensity method as follows [7]:

$$t = \lambda \ln (I_t / I_0)$$

where I_0 and I_t are the integrated intensities in the zero loss peak and the total intensity in the spectrum, respectively. The mean free path of inelastic scattering λ was calculated from the energy dependence of the low-loss spectrum, utilizing a Kramers-Kronig sum rule [7].

3.2 DECONVOLUTION OF THE SPECTRA. — Although the analyzed specimen regions were thinner than a half of the mean free path for inelastic scattering (λ), all spectra had to be deconvoluted to remove all plural-scattering features before background subtractions and quantifications. This was done by means of the Fourier-log method [7] which improves the edge-to-background ratio and the background in front of the edges thus making background subtractions more reliable.

However, it is worth noting that for a perfect deconvolution there should be good linearity in the electron counting system, uniform sample thicknesses as well as a very large collection angle [18]. On the other hand we have to use small collection angles to get a good peak-to-background ratio in the low loss-region. Therefore, we have to make a compromise choosing a medium collection angle of 7.6 mrad. Experimental results [19] indicate that the Fourier-log-method is accurate to better than 3% in the low-loss region, for apertures commonly used in a TEM. Since deconvolution artifacts increase in case of thicker samples [7], spectra were always collected from specimen regions not thicker than about 0.5 λ. Additionally the spectra have been taken from specimen regions whose thicknesses have been only slowly varying. From figure 1 the effect of deconvolution can be deduced. Figure 1a shows the low-loss spectrum of phenacite (Be_2SiO_4) with the Be K and the Si L_{23} edges taken from a thin specimen region, where the t/λ ratio was about 0.38 thus giving a specimen thickness of about 57 nm. Although plural-scattering effects are not observable, deconvolution of this spectrum (Fig. 1b) improves the visibility of the edges essentially.

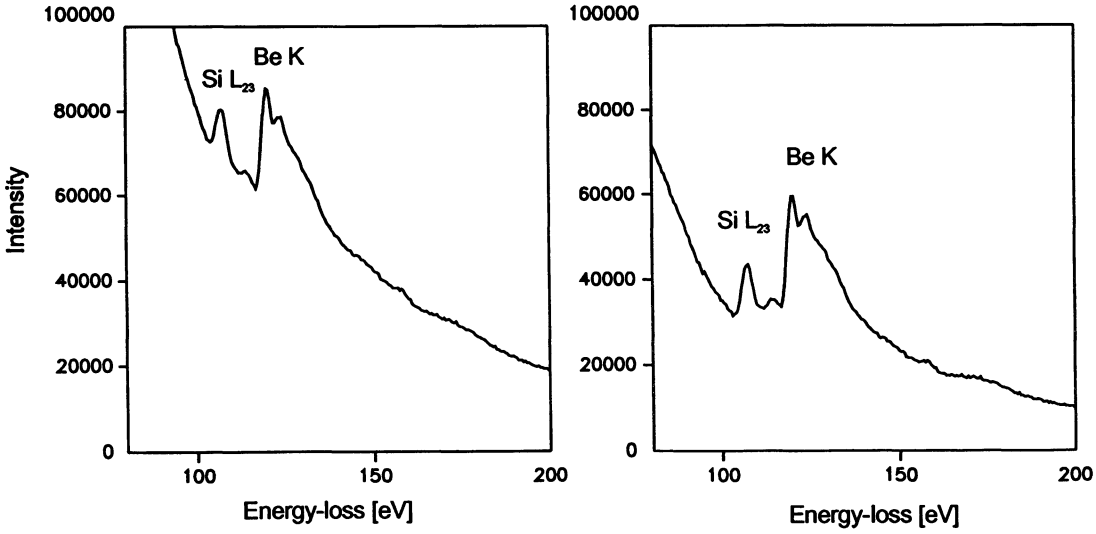

Fig. 1. — EEL spectrum of phenacite (Be_2SiO_4); a) original spectrum ($t/\lambda = 0.38$); b) deconvoluted with the Fourier-log-method.

3.3 BACKGROUND SUBTRACTION. — The background extrapolation is very important for correct extraction of the integrated intensities. Backgrounds below the edges were determined by fitting the usual $A \cdot E^{-r}$ curve to a selected background region just ahead of the edge: In case of the low-loss edges only 20-30 eV windows can be used and 50 to 70 eV for the high loss edges. Due to the low edge to background ratio in the low loss region, background has to be carefully modelled otherwise Li and Be quantifications will become inaccurate. However, if the spectra have been recorded from thin specimen regions (see Sect. 3.2) and subsequently deconvoluted, the conventional background extrapolation yielded reliable results, as it can be deduced from the quantification results.

In case of Cr containing oxides, background subtraction under the Cr M_{23} edge leads to erroneous results, i.e. the extrapolated background rises above the spectrum. Therefore an alternative method has been used: The background below the Cr M_{23} edge has been fitted by a linear least square fit of the function $A \exp(-rE)$ in a log-lin transformed spectrum (Fig. 2) [20].

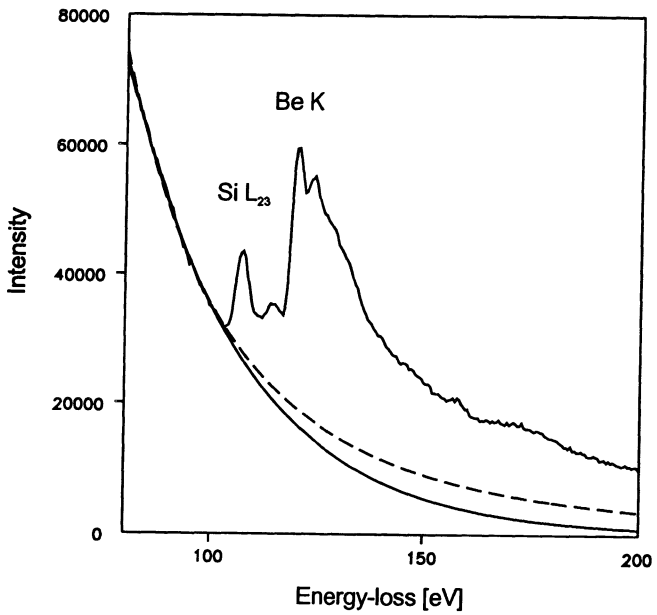

Fig. 2. — EEL spectrum of phenacite (deconvoluted); Background subtraction with the conventional $A \cdot E^{-r}$ model (dashed line) and with a log-lin model (solid line).

3.4 MLS-FIT OF OVERLAPPING EDGES. — As already discussed, a great limitation to EELS analysis is that imposed by overlapping peaks. Edge intensities then can only be determined by separating edges using a set of reference spectra fitted to the unknown by a multiple - least - squares (MLS) algorithm. This method is similar to that used in the analysis of energy-dispersive X-ray spectra.

Such a procedure for the application in EEL spectrometry has been first proposed by Shuman and Somlyo [21]: Here the background underlying the group of edges was removed by

computing the first difference spectrum so that the slowly varying background is strongly suppressed. Provided the reference spectra are treated similarly, they can be fitted directly to the unknown spectrum. Leapman and Swyt have demonstrated that this method can be applied to undifferentiated spectra as well, if the intensity in front of the group of edges is extrapolated and subtracted in the conventional way [22]. A similar approach has been used by Manoubi *et al.* [23].

The spectrum with the overlapping edges is quantified by a multiple least squares fit to reference spectra. If the k^{th} reference spectrum is labelled $X_k(E_i)$ where $k = 1$ to M, then the fitting coefficients a_k are determined by minimizing the value of χ^2,

$$\chi^2 = \frac{\sum_{i=1}^{N} \left[I(E_i) - \sum_{k=1}^{M} a_k * X_k(E_i) \right]^2}{[\sigma(E_i)]^2} = \text{Minimum}$$

$I(E_i)$ is the intensity recorded at the i^{th} channel ($i = 1$ to 1024) at energy-loss E_i and $\sigma(E_i)$ is the standard error in the i^{th} channel of the unknown spectrum. The method used here for the MLS fitting is the singular value decomposition technique (SVD) [24] which has been proposed recently by Leapman and Hunt [25].

The reference spectra - thin film standards have been used - have been measured under identical conditions like the unknown spectra. They have to be treated in a similar way, i.e. Fourier-log-deconvolution and conventional background subtraction. Deconvolution of either references and unknown is necessary in our approach, because plural inelastic scattering changes the edge shapes and the MLS-fit can fail. Another possibility to consider plural scattering has been proposed by Leapman and Swyt [22]. In this case the single scattering reference edges are additionally convoluted with the low loss spectrum of the unknown. However, in case of the low loss edges our technique seems to be more useful because the Fourier-log-deconvolution not only improves the behaviour of the background below the edges but also enhances the visibility of edges. This has an favourable effect especially on the low loss region, where edge to background ratios are generally very small.

The MLS method was derived on the assumption that edge profiles are the same in the unknown and in the reference. Since variations in chemical bonding can significantly modify edge fine structures [26], we have to use standards with similar chemical bondings. Fortunately, it is well known that the nearest neighbours of the element (coordination) that gives rise to an ionization edge determine its near-edge fine structure (ELNES) [26, 27]: Therefore, the L_{23} or K edges exhibit typical edge shapes (fingerprints) e.g. for Al [27, 28] or Si [27, 29] in octahedral or tetrahedral coordination with oxygen atoms. To apply the MLS-fit to oxides and silicates, we only have to use oxide standards with elements of identical coordination. Thus we made use of corundum (α-Al_2O_3), quartz (α-SiO_2), BeO and $Ca_3(PO_4)_2$ as reference materials.

Since the quality of the fit is also a function of energy-loss calibration of the unknown spectrum with respect to the references, quite large errors can occur even if there is a miscalibration of 1 eV. To correct these miscalibrations, the MLS program used by us has got a procedure which allows to shift the references relatively to the edge thresholds of the measured spectrum. This feature essentially improves the fit of the unknown spectrum.

3.5 QUANTIFICATION. — The atomic concentration ratio N_A/N_B of any elements A and B may be determined from an EEL spectrum using the following equation [30, 7],

$$\frac{N_A}{N_B} = \frac{I_A(\beta, \Delta)}{I_B(\beta, \Delta)} \cdot \frac{\sigma_B(\beta, \Delta)}{\sigma_A(\beta, \Delta)}$$

where

- N_i is the number of atoms per unit area
- $I_i(\beta, \Delta)$ is the core loss intensity integrated up to an energy region of width Δ starting at the edge onset
- $\sigma_i(\beta, \Delta)$ is the partial ionization cross-section integrated over the acceptance angle β and an energy region Δ.

A typical value for Δ in the low energy region lies within 30 to 50 eV and should be used, hence optimizing the edge to background ratio and minimizing background extrapolation errors. The partial cross-sections were calculated using the hydrogenic model [7] (see Tab. I). Since these calculated cross-sections should be used with caution if integrated over small energy regions, we additionally used experimentally determined k-factors. These k -factors can be easily used instead of cross-sections, since they are cross-section ratios which are measured relatively to the K edge of oxygen, e.g. for the element A:

$$k_{A,O} = \frac{\sigma_O(\Delta, \beta)}{\sigma_A(\Delta, \beta)}$$

The k-values for the K and L_{23}-edges were evaluated using the corresponding oxides as thin film standards according to the procedure previously described [16]. In case of Li we used LiF and the k-factor was converted from F into O ratios by using hydrogenic cross-sections. These values (in Tab. I) are quite similar to k-factors that have been recalculated from previously published measurements at 120 kV [16]. The k-factor for the Cr M_{23}-edge was taken from [31].

Table I. — *Partial cross-sections and k-factors for the ionization edges which have been used for the quantifications. Experimental conditions:* $E_0 = 200$ kV, $\beta = 7.6$ mrad, $\alpha < 1.5$ mrad.

Edge	Δ [eV]	Exp. k-factors * 10^{-3}	Exp. cross-sections [cm^2/atom]	Hydrogenic model [cm^2/atom]
Li K	30	9.0 ± 1.2	5.30 E-20	7.19 E-20
	50	10.7 ± 1.5	6.97 E-20	8.58 E-20
Be K	50	40.5 ± 1.3	1.84 E-20	2.26 E-20
Al L_{23}	50	12.5 ± 1.5	5.95 E-20	7.46 E-20
Si L_{23}	50	17.7 ± 1.4	4.20 E-20	4.50 E-20
P L_{23}	50	25.8 ± 4.3	2.88 E-20	3.05 E-20
Cr M_{23}	30	2.77 ± 0.25	1.73 E-19	3.30 E-20

4. Results and discussion.

4.1 Li COMPOUNDS. — The Li K edge is a rising edge at 55 eV, superimposed on the tail of the plasmon peak. Figure 3 shows the energy-loss spectra of Li compounds like LiF, Li_2O, spodumene ($LiAl[SiO_3]_2$) and lepidolite ($K_2Al_3Li_2[AlSi_7O_{20}](OH)_2F_2$). The oxygen and fluorine K edges

are not included since they are similar to that of Al_2O_3 [32]. Although these spectra have been recorded from very thin specimen regions, the edge-to-background-ratio is low due to the vicinity of the plasmon peak.

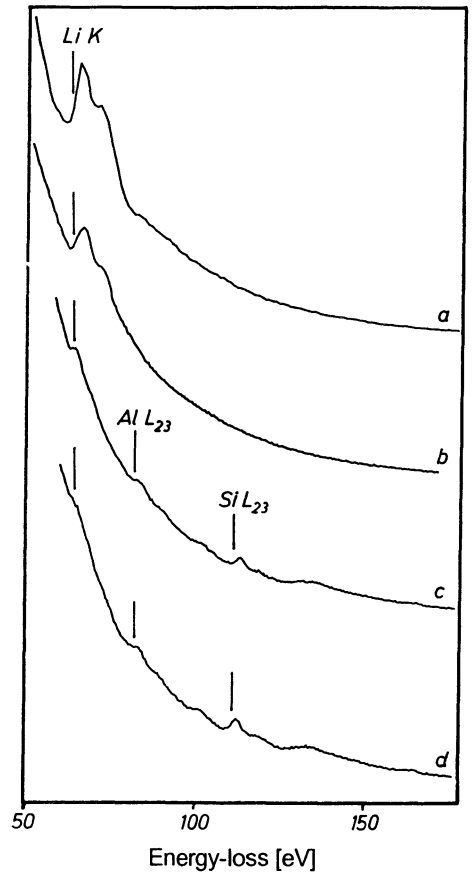

Fig. 3. — EEL-spectra of some Li compounds; a) LiF (50at% Li); b) Li_2O (66.6at% Li); c) spodumene ($LiAl(SiO_3)_2$) (10at% Li); d) lepidolite ($K_2Al_3Li_2[AlSi_7O_{20}](OH)_2F_2$) (4.9at% Li).

In spodumene and lepidolite the Li K edge overlaps with the L_{23} edges of Si and Al. Despite the low concentration of Li in these compounds the Li signal is easily detectable, because the Li K edge rises at lower energies than the L_{23}-edges. However, more problems arise with the detection of Li in Li-Cr-oxide, because the Cr M_{23} edge interferes with the Li K edge. It can only be identified by comparison with well known reference edges (see Fig. 5).

It has been long known that the L_{23} edges of Al and Si exhibit chemical shifts when changing the chemical state going from the metal to an insulator (e.g. oxide). In this case the band gap shifts the edge to higher energy-loss [26]. The threshold energies of these L_{23}-edges are raised in case of Al from 73 to 78 eV and in case of Si from 99eV to 105 eV (Tab. II). Similarly the Li K edge also exhibits a chemical shift when going from the metal to insulating oxide compounds. For the Li minerals (Fig. 3) the threshold energy of the Li K edge is raised from 55 eV to 59 eV.

Table II. — *Chemical shifts of some low energy edges in pure elements and in oxide compounds; threshold energies in* eV *with an error of* ±0.5 eV.

Edge	Element	Oxide
Li K	55	59
Be K	111	117
Al L_{23}	73	78
Si L_{23}	99	105
P L_{23}	132	136
Cr M_{23}	42	45

Owing to the high volatility of Li at room temperature (similar to Na and K), we always found that the Li signal decreased between successive measurements on the same specimen regions. However, the loss of Li is almost completely avoided if the specimens were cooled to 70 K. Additional spectra for quantitative work have been recorded from specimen regions that have not been irradiated previously.

Quantification of spodumene ($LiAl[SiO_3]_2$):

Spodumene is not only a typical representative for Li-minerals but also for breeder materials for nuclear fusion (Li-silicates and aluminates). The quantitative microanalysis of Li in this class of compounds is therefore very important and is readily performed by using EELS: Figure 4a shows the relevant region of the energy-loss spectrum of spodumene with the edges Li K, Al L_{23} and Si L_{23} ($t/\lambda = 0.43$). This spectrum has been deconvoluted to improve the visibility of the edges. The background was modelled using the conventional $A \cdot E^{-r}$ model with a fitting region of 20 eV immediately in front of the Li K edge (40 to 58 eV). The fitting region must not be wider than this value, because the vicinity of the plasmon peak deteriorates the background below energy-loss values of 35 eV. The MLS-fit was performed with the background function and the reference edges from LiF, α-Al_2O_3 and α-SiO_2. The modelled spectrum is shown in figure 4a. The spodumene spectrum is fitted quite well using the reference edges, provided the fine structure details close to the onset of the Li K edge are ignored. To quantify the spectrum from figure 4b the intensities of the reference edges were integrated within 50 eV above the edge onset. The atomic ratios for Li/Al and Al/Si were determined from 7 spectra which have been recorded from specimen regions of different thicknesses ($t/\lambda = 0.4$-0.7). Quantification results are represented in table III. While the Li/Al and Al/Si ratios are in good agreement with the nominal values using experimentally determined k-factors, it can be seen that, if hydrogenic values were used instead, more significant deviations especially in the Li/Al ratio occur which can be mainly attributed to the Li cross-sections.

Quantification of Li-Cr-oxide :

This compound stands for the Li-transition metal oxides which are of great scientific and technological importance. However, these oxides are difficult to prepare for AEM investigations, because they are often very soft and - if ion milled - lithium may be lost. Therefore, we have used

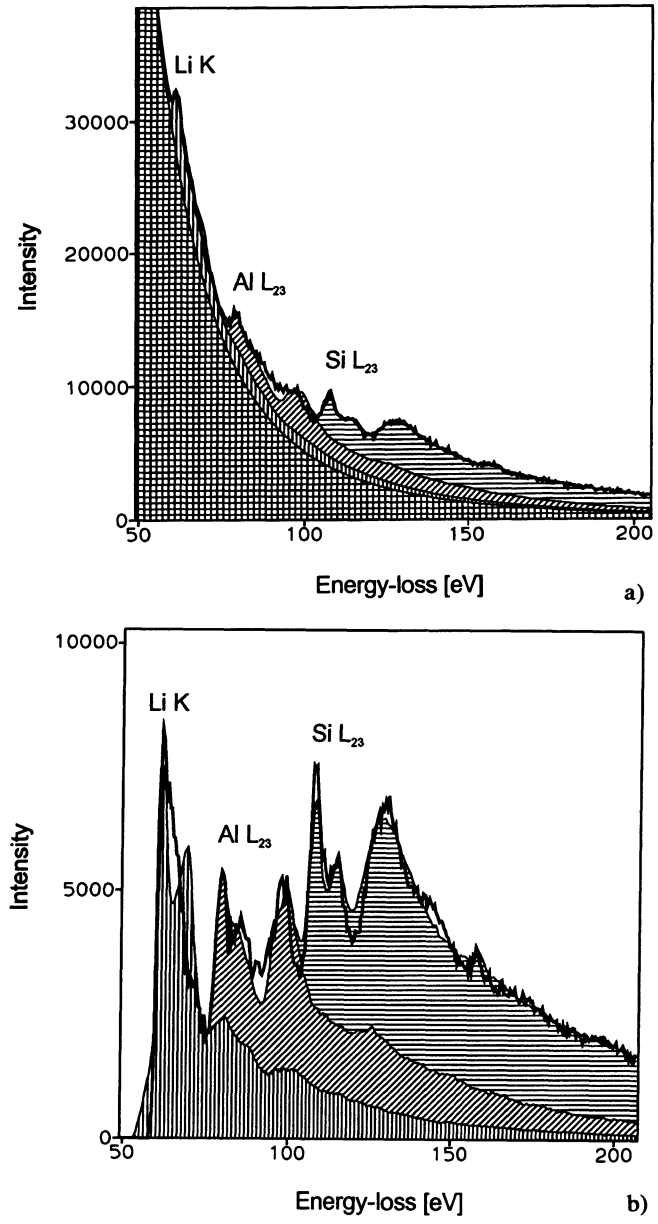

Fig. 4. — EEL spectrum of spodumene with overlap of the LiK, Al L_{23} and Si L_{23} edges; recorded at 80 K; MLS fit with reference edges; a) deconvoluted spectrum; b) deconvoluted spectrum with subtracted background.

small single crystals that have been crushed under liquid nitrogen.

The quantitative EELS-analysis of these compounds is complicated by the M_{23} -edges of the first row transition metals which overlap with the Li K edge. Figure 5a shows the relevant area of the energy-loss spectrum of $LiCrO_2$ with the edges Cr M_{23} and Li K. The spectrum is already deconvoluted and the background beyond the Cr M_{23}-edge could only be fitted by the log-lin model which has been previously used with the Cr M_{23}-edge in Cr_2O_3 [31]. Like in spodumene the near

Table III. — *Results of EELS quantifications of Li-compounds: The atomic ratios have been determined using either experimentally determined k-factors or calculated cross-sections (hydrogenic model). Experimental conditions:* $E_0 = 200kV$, $\beta = 7.6$ mrad, $\Delta = 50$ eV*; average values for 5 or 7 spectra with standard deviation.*

		Nominal	Exp.k-factors	Hydr. model
Spodumene	Li/Al	1.0	1.08 ± 0.10	1.12 ± 0.10
	Al/Si	0.5	0.496 ± 0.10	0.426 ± 0.08
$LiCrO_2$	Li/Cr	1.0	0.94 ± 0.12	0.132 ± 0.02

lying plasmon peak has got a great influence on the background fit and therefore only small fitting regions of 15 - 20 eV immediately below the Cr M edge were used. The MLS-fit was performed with the reference edges from LiF and Cr_2O_3 and as figure 5b shows, satisfactory agreement exists between the Li-Cr-oxide spectrum and the modelled spectrum. A small window of 30 eV was chosen for the determination of the edge intensities, since Li K and M_{23} edges concentrate almost all intensity within a window of 30 eV. The quantification result is presented in table III. If the Li/Cr ratio is determined using experimental *k*-factors, it is very close to the nominal ratio. However, quantification with the hydrogenic values results in relatively large deviations from the nominal composition which can be mainly attributed to the calculated cross-section of the Cr M_{23} edge. It has recently been shown that this model cannot predict the M_{23}-edges adequately [31] and that the best solution to this problem is to use experimentally determined cross-sections.

4.2 Be COMPOUNDS. — Figure 6 shows the EEL-spectra of Be compounds like BeO, phenacite (Be_2SiO_4), chrysoberyl (Al_2BeO_4) and beryl ($Al_2Be_3Si_6O_{18}$). The oxygen K edges of the minerals resemble to that of Al_2O_3 [32], therefore they are not included. Although these spectra have been recorded from very thin specimen regions, the peak-to-background ratio is low due to the vicinity of the plasmon peak.

In phenacite and chrysoberyl the Be K edge overlaps with the Si L_{23} edge or with the Al L_{23} edge and is easily detectable due to the comparatively high Be concentration in these compounds. However, more problems arise with the detection of Be in beryl, because both L_{23} edges overlap with the Be K edge. Here the Be concentration is rather low and therefore the small Be edge is rather difficult to identify in the original spectrum (Fig. 6). It can only be found by careful data reduction in comparison to well known reference edges (see Fig. 8). Similar to the Li K edge in oxidic compounds, the Be K edge exhibits also a chemical shift when going from the metal to the oxide. The threshold energy of the Be K edge is raised from 111 eV in the metal to 117 eV in BeO and this shift occurs in the other Be minerals too (Tab. II).

In case of the investigated Be compounds no loss of Be could be observed and therefore the measurements could be performed at room temperature.

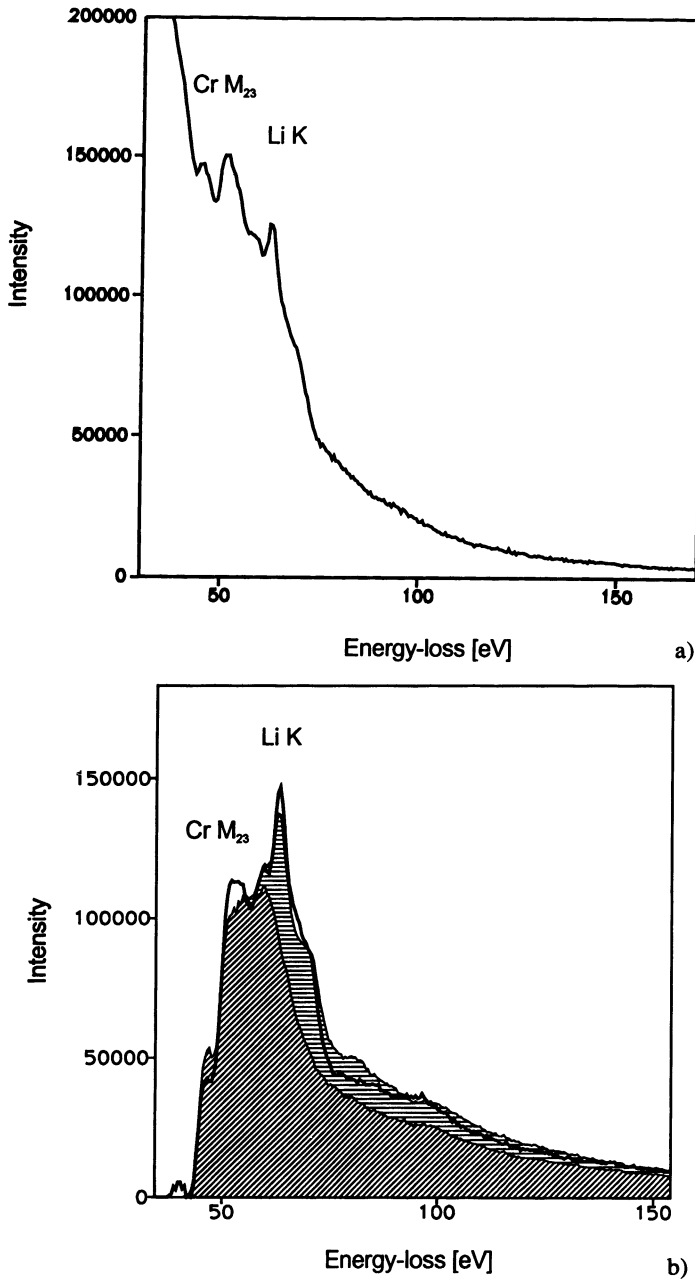

Fig. 5. — EEL spectrum of $LiCrO_2$ with overlap of the Cr M_{23} and the Li K edges; recorded at 80 K; a) deconvoluted spectrum; b) MLS fit of a background subtracted edge group with reference edges.

Quantification of phenacite (Be_2SiO_4):

Figure 7a shows the relevant region of the energy-loss spectrum of phenacite with the edges Si L_{23} and Be K. This spectrum has already been deconvoluted to improve the visibility of the edges (compare with Fig. 1). The background was modelled making use of the inverse power-law

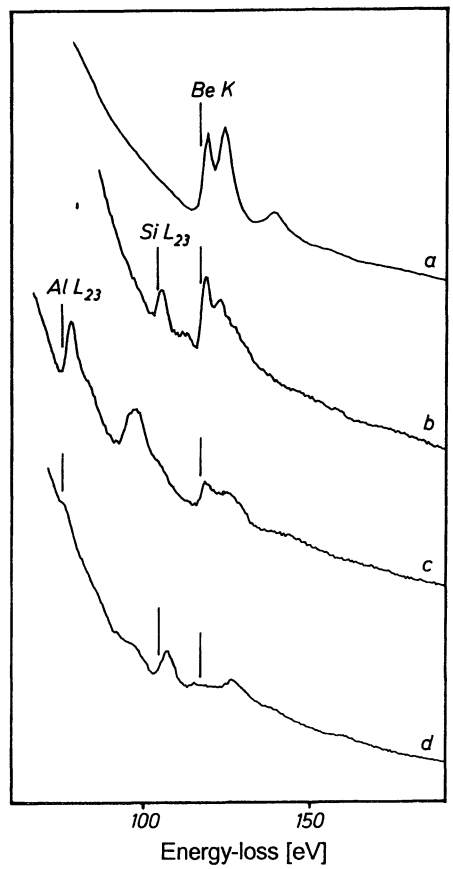

Fig. 6. — EEL-spectra of some Be compounds; a) BeO (50at% Be); b) phenacite (Be_2SiO_4) (28.6at% Be); c) chrysoberyl (Al_2BeO_4) (14.3at% Be); d) beryl ($Al_2Be_3Si_6O_{18}$) (10.3at% Be).

$A \cdot E^{-r}$ model with a fitting region of 30 eV immediately ahead of the Si L_{23} edge. The MLS-fit was performed with the reference form α-SiO_2 and BeO and the result is shown in figure 7b. it is obvious that the Si L_{23} -edge is modelled quite well, but the Be K edge exhibits significant differences of fine structure between both compounds. To quantify the spectrum from figure 7a the intensities of the reference edges were integrated within 50 eV above the edge onset. The quantification result is shown in table IV clearly proving that experimental k-factors give better agreement with the nominal concentration ratio than the hydrogenic values.

Quantification of beryl ($Al_2Be_3Si_6O_{18}$):

Figure 8a contains the relevant region of the energy-loss spectrum of beryl with the edges Al L_{23}, Si L_{23} and Be K. The spectrum has been deconvoluted as well. The background fitting was more difficult than in the previous example, since the Al L_{23} edge is nearer to the plasmon peak. Therefore the background before the Al L_{23} edge could only be fitted within some 25 eV. Despite this very small fitting region the conventional $A \cdot E^{-r}$ model was again applied and reliable results could be obtained. The MLS fit was performed with the $A \cdot E^{-r}$ background and reference edges from α-Al_2O_3, α-SiO_2 and BeO. While the Al and Si edges are clearly visible and also fitted

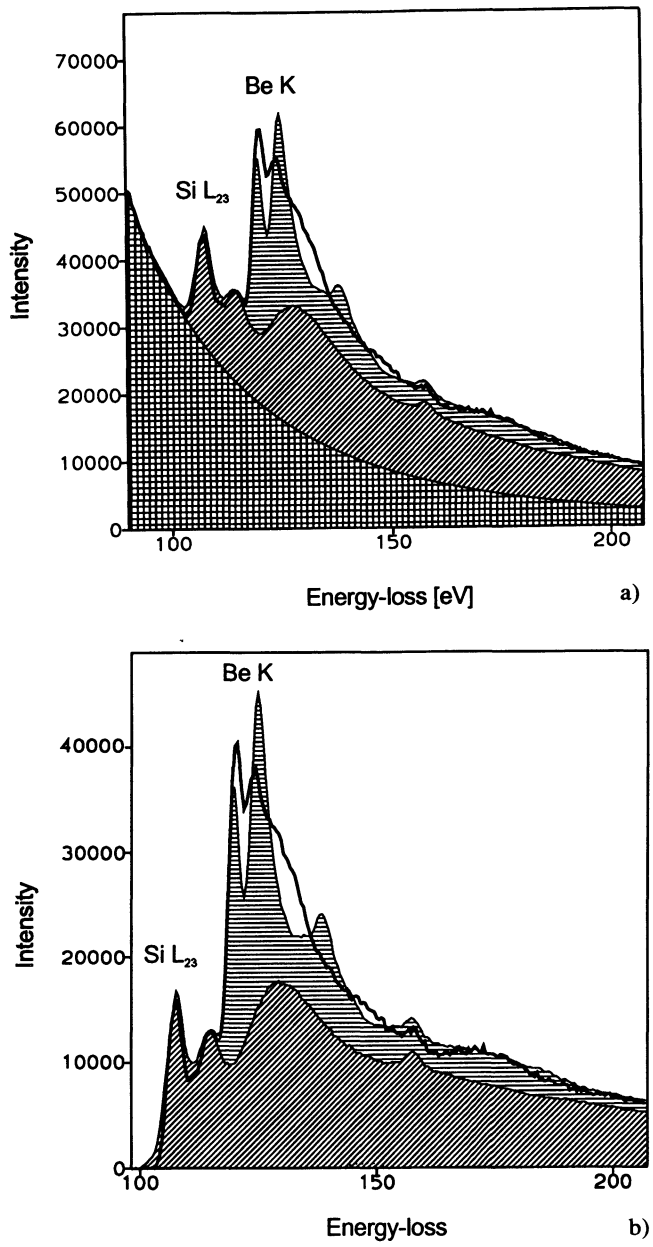

Fig. 7. — EEL spectrum of phenacite with overlap of the Si L_{23} and Be K edges; MLS fit with reference edges; a) deconvoluted spectrum; b) deconvoluted spectrum with subtracted background.

quite well, the Be K edge is only unequivocally identified by the MLS-fit approach. This dues to the relatively small Be concentration in this compound (5 wt% Be) and additionally the edge-to-background ratio for the Be K edge is low, since the Al and Si L_{23} edges are contributing to the Be K edge's background. The intensities were integrated within a 50 eV window above edge onset

Table IV. — *Results of EELS quantifications of Be-compounds: The atomic ratios have been determined using either experimentally determined k-factors or calculated cross-sections (hydrogenic model). Experimental conditions:* E_0 = 200kV, β = 7.6 mrad, α = 1.5 mrad, Δ = 50eV; *average values for 5 spectra with standard deviation.*

		Nominal	Exp. k-factors	Hydr. model
Phenacite	Be/Si	2.00	1.89 ± 0.12	1.65 ± 0.11
Beryl	Be/Si	0.50	0.49 ± 0.05	0.43 ± 0.04
	Al/Si	0.33	0.31 ± 0.04	0.266 ± 0.03
Weinebeneite	Be/P	1.50	1.34 ± 0.05	1.15 ± 0.04

and the concentration ratios are in relatively good agreement with the nominal composition (Tab. IV).

We have also tried to quantify beryls with small amounts of Mg and in this case we did not succeed. The fact that the Mg L_{23} edge which is situated at 52 eV additionally overlaps with the other three edges, augmented the problems concerning background fitting and extrapolation. Therefore it was not possible to quantify these compounds.

Quantification of weinebeneite ($Be_3Ca(PO_4)_2(OH)_2 \cdot 4H_2O$):

Weinebeneite is a new Be-mineral which has recently been found in the Styrian mountains [33]. Besides the crystallographic characterization by X-ray diffraction the mineral has been thoroughly analyzed in the electron microprobe using wavelength dispersive X-ray spectrometry [34]. Weinebeneite was found to consist mainly of Ca, P and O and chemical analysis suggested the occurrence of light elements like Li or Be. Therefore we additionally used EELS to detect and quantify the light elements. Due to the lack of material - only some crystals have been found - crystals were crushed and mounted on holey carbon film supported grids.

A typical EEL-spectrum recorded from weinebeneite (Fig. 9) clearly shows the detection of Be, P, Ca and O as major constituents. Li could not be identified in the spectrum, although digital filtering leading to first- and second-order derivatives was tried to enhance the visibility of minor constituent edges. Due to the high water content the specimen rapidly decomposed under electron irradiation and therefore the specimen had to be cooled to a temperature of 70 K.

To quantify Be we have to consider that the Be K edge overlaps with the P L_{23} edge. Figure 10a shows the relevant region of the Fourier-log deconvoluted spectum with the Be K and P L_{23} edges. The background in front of the Be K edge was fitted within some 30 eV by the inverse power-law model and the MLS-fit was performed with reference edges from BeO and $Ca_3(PO_4)_2$. As figure 10b shows, a satisfactory fit is again achieved, provided the near edge fine structure of the Be K edge is ignored. The measured Be/P atomic ratio of 1.34 ± 0.05 (using experimental k-factors) agrees with the nominal Be/P-ratio of 1.5 which has been deduced from X-ray diffraction investigations [34].

4.3 DETECTION LIMITS. — EELS offers advantages in detection efficiency of light elements in comparison to EDX-spectrometry. Furthermore the partial cross-sections for Li and Be K ionizations are very high thus leading to high intensities of Li and Be K edges when compared to other EELS edges. On the other hand the edge-to-background ratios are extremely small due to the vicinity of the intense plasmon peak and due to plural scattering both influencing the energy-loss region more than the high energy-losses (above 150 eV) even in thin specimens. When consider-

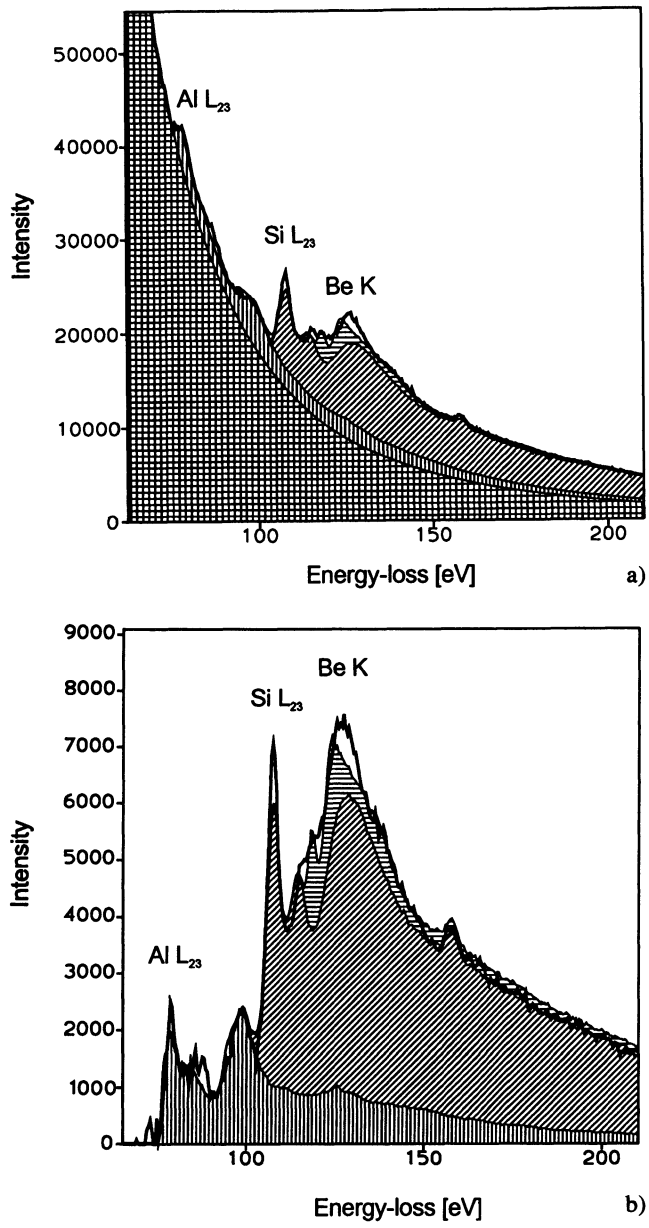

Fig. 8. — EEL spectrum of beryl with overlap of the Al L_{23}, Si L_{23} and Be K edges; MLS fit with reference edges; a) deconvoluted spectrum; b) deconvoluted spectrum with subtracted background.

ing the sensitivity of a microanalysis, however, it is the peak-to-background value rather than the net intensity of the edge that is of significance.

As already mentioned the Li and Be K edges often overlap with other edges. Then we have to differentiate between two situations. In the first case the Li or Be edge is not overlapping with other edges or the overlapping edge is occuring at higher energy-losses than the Li or Be

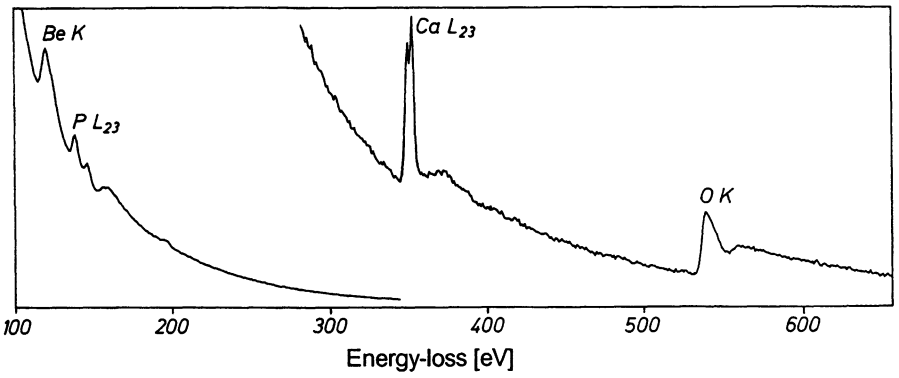

Fig. 9. — EEL spectrum of weinebeneite with the overlapping Be K and P L_{23} edges and with the Ca L_{23} and O K edges ($t/\lambda = 0.44$).

K edge (e.g. Li K and Al L_{23}) thus giving good detection possibilities for Li or Be. However, if the overlapping edge occurs at lower energy-losses than the Li or Be edge, the overlapping edge contributes to the background and thus severely deteriorates the detection limits of Li or Be (e.g. Si L_{23} and Be K). The elements which give rise to edges occurring at lower energy-losses than the K edges of Li and Be are summarized in table V.

Table V. — *Summary of elements which decrease the detection sensitivity for Li and Be, because the ionization edges of these elements occur at lower energies than the Li and Be K edges.*

Li K edge		Be K edge	
Element	Edge	Element	Edge
Na, Mg	L_{23}	Al, Si	L_{23}
Ca - Co	M_{23}	Se - Sr	M_{45}
Ge, Se	M_{45}	Pd - In	N_{23}
Sr - Cd	N_{23}	Te - Nd	N_{45}
Sn - I	N_{45}	Th, U	O_{45}
Hf - Ir	O_{23}		

In this work we estimate the minimum mass fractions (MMF) of Li and Be in silicates by using an experimental approach which was first proposed by Isaacson and Johnson [35]. We have collected our data using a serial EEL-spectrometer and of course one may expect better sensitivities by using a parallel spectrometer (PEELS). Nevertheless, the sensitivities of Li and Be are mainly governed by the high backgound. By analyzing relatively large areas ($\sim 0.1\ \mu m^2$) we obtain spectra with high count rates comparable to parallel recorded spectra (in the low loss region). The signal-to-background ratios of the edges of interest are measured from a deconvoluted spectrum.

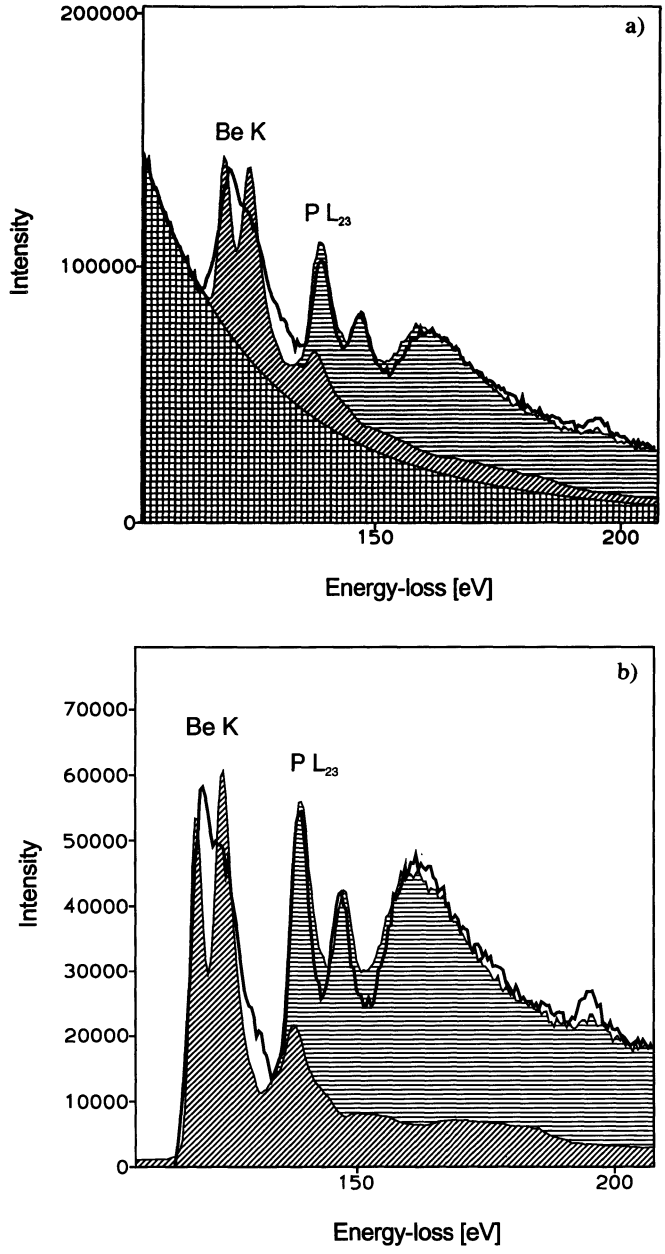

Fig. 10. — EEL spectrum of weinebeneite with overlap of the Be K and P L_{23}-edges; a) MLS fit with reference edges of a deconvoluted spectrum. b) deconvoluted spectrum with subtracted background.

The signal-to-noise ratio (SNR) is calculated by

$$SNR = \frac{I_k}{(I_k + hI_b)^{1/2}}$$

in which I_k and I_b are the intensities of core loss and background, respectively, and the factor h

represents statistical errors of background extrapolation [7]. If $SNR \propto I_k \propto x$, where x is the atomic mass fraction of the element giving rise to the edge, x_{min} is calculated as the value of x for which SNR equals 3 (98% certainty for detection of the element) [7]. Since the main intensity of the Li and Be K edges is concentrated at the edge onset, we used integration regions of 15 eV for the determination of background and edge intensities. The MMF of Li has been evaluated using a deconvoluted spodumene spectrum. If the factor h is considered ($h = 50$), a MMF - value of about 2 at% Li could be determined, and with $h = 0$ we get an MMF of 0.4 at% Li. To derive the corresponding figure for Be, a spectrum of weinebeneite has been used thus yielding a MMF of 0.3 at%. In case of overlapping edges these figures are increased towards the 1 at% range. If, for example, the Be K edge overlaps with the Si L_{23} edge and Be is minor constituent, the Be K edge is hidden in the near edge fine structure of the Si L_{23} edge and then Be is extremely difficult to detect (see Beryl). A similar situation occurs if the Mg L_{23} edge overlaps with the Li K edge (Fig. 11).

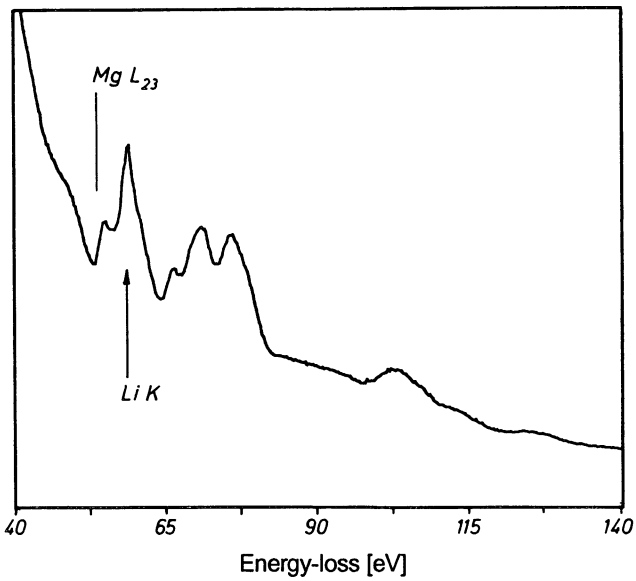

Fig. 11. — EEL spectrum of the L_{23} edges in MgO; the arrow indicates the position of Li K edge.

Using similar arguments, Joy and Maher [36] deduced the minimum detectable concentrations of Li and Be in a carbon and silicon matrix and found MMF values between 0.02 and 1 at%. Leapman investigated the detection limits of various elements in a glass matrix using a microscope operated with a field-emission gun and a PEELS-system [37]. The elements Li (0.153 at%) and Be (0.118 at%) were not detectable, although second-difference spectra have been recorded to enhance the visibility of the edges.

Thus we may expect that it will be difficult to improve the minimum detectable concentrations for Li and Be which are ranging from 0.5 - 2 at%. This is mainly due to the low edge-to-background ratios of these edges.

5. Discussion.

We have demonstrated the principle possibility of quantifying Li and Be in oxides even in case of severe overlaps with L_{23}, M_{23} edges or other low energy edges. The EELS-quantifications agree with the nominal composition of the test compounds within 20 rel%.

The errors in the quantifications are represented by the standard deviations of our measurements made on 5 to 8 different specimen areas with different thicknesses in each case. The measurement errors come from two sources, statistical and systematic ones. The main uncertainty is caused by the background subtraction errors which contain on the one side a systematic error if the background deviates from the assumed form, and on the other side a statistical error due to extrapolation. In this work, the only source of error that could be estimated was the statistical one.

One problem of these quantification procedures is that the integration range was always greater than the small pre-edge background fitting region. Additionally, we sometimes have to extrapolate the background very far above the pre-edge fitting region. The worst situation in this respect is the quantification of Li and Si in spodumene. To determine the Si L_{23} intensity we have to extrapolate from a 15 or 20 eV wide fitting window below the Li K edge to about 150 eV. However, even in this case we find good agreement between nominal and measured compositions thus confirming that the conventional background model works quite satisfyingly. If the background function is included in the MLS-fit, better quantification results could be obtained, because the values A and r are constrained to be acceptable over the total energy range of interest rather than only in front of the edges.

It has been shown previously [23] that calculated edge shapes can be used for the fit of overlapping edges. We have tried to use edge profiles calculated by the hydrogenic model, but this approach has not been successful, because the edge fine structures are not considered. In case of Li and Be compounds the edges overlap within the near edge region and therefore theoretical edge shapes have to be replaced by reference edges. The simplicity of the MLS method depends on the assumption that the core edges are the same in the unknown and reference. Such effects can be fully taken into account if reference edges are used that have been obtained from compounds where the element of interest has very similar chemical environment.

One source of systematic errors in EELS quantifications is still that of the partial cross-sections for inner-shell ionizations. The foregoing results show that calculated cross-sections yield satisfying quantification results for the K and L_{23}-edges of the light elements, but not for M_{23} or N_{45}-edges. However, for accurate quantifications we recommend the use of experimentally determined k-factors or cross-sections. These values have been already measured for most elements and for K, L_{23}, M_{45}, N_{45} and M_{23}-edges and have been compiled recently [16, 38].

6. Conclusions.

The procedures required for quantification of Li and Be in oxides and silicates by using EELS in a TEM/STEM have been examined thoroughly:

1) The specimen regions, within the EEL-spectra are to be measured, should be as thin as possible ($t/\lambda < 0.5$) and to enable reliable background subtractions the spectra have to be deconvoluted using the Fourier-log-method. Then the conventional $A \cdot E^{-r}$ model can be applied successfully in most cases.
2) Li and Be K edges overlap with L_{23} and M_{23}-edges very often. Thus the edges have to be separated by using a MLS-fit with reference edges which have been recorded from standards

with similar chemistry.

3) It has been shown that accurate quantification results can be obtained if experimentally determined k-factors are used for the K, L_{23} and M_{23}-edges. However, the usage of calculated cross-sections leads to significant deviations from the nominal concentrations up to $\pm$ 50 rel%.
4) Since Li is very volatile, heavy mass losses have been found during investigation at room temperature. Therefore measurements of Li compounds had to be performed at a temperature of 70 K. In case of Be compounds no loss of Be was detectable.
5) Furthermore one has to consider that both Li and Be K edges exhibit a positive chemical shift of some eV in oxides and silicates when compared with the metallic samples.
6) Detection limits of Li and Be have been determined to be in the 1 at% range. However, if the K edges of Li and Be overlap with the L_{23} edges of Na to Si the detection limits increase to about 1 to 3 at% .

Acknowledgements.

We are very grateful to Prof. Dr. H.P. Fritzer, Dr. A. Popitsch, Dr W. Postl, J. Taucher and Dr. F. Walter for providing test samples. We gratefully acknowledge financial support by the Forschungsförderungsfonds der Gewerblichen Wirtschaft, Vienna.

References

[1] DISKO M.M., AHN C.C., FULTZ B., Transmission Electron Energy Loss Spectromety in Materials Science. TMS, The Minerals, Metals & Materials Society (1992).
[2] ARMIGLIATO A., BENTINI G.G., RUFFINI G., *J. Microsc.* **108** (1976) 31.
[3] L'ESPERANCE G., BOTTON G., CARON M., Microbeam Analysis-1990, Michael J.R., Ingram P. Eds., San Francisco Press Inc. (San Francisco, 1990) p. 284.
[4] LIU D.R., WILLIAMS D.B., Microbeam Analysis-1986, Romig A.D., Chambers W.F. Eds., San Francisco Press Inc. (San Francisco, 1986) 425.
[5] LIU D.R., WILLIAMS D.B., *Proc. R. Soc. Lond.* **A 425** (1989) 91.
[6] LIU D.R., WILLIAMS D.B., *J. Microsc.* **156** (1989) 201.
[7] EGERTON R.F., Electron Energy-Loss Spectroscopy in the Electron Microscope. (Plenum Press, New York & London, 1986).
[8] LIU D.R., WILLIAMS D.B., Proc. 45th Ann. EMSA Meeting, Bailey G.W. Ed., San Francisco Press Inc. (San Francisco, 1987) p. 118.
[9] WILSON A.R., *Microsc. Microanal. Microstruct.* **2** (1991) 269.
[10] TENAILLEAU H., MARTIN J.M., *J. Microsc.* **166** (1992) 297.
[11] LEAPMAN R.D., REZ P., MAYERS D.F., *J. Chem. Phys.* **72** (1980) 1232.
[12] REZ P., *Ultramicroscopy* **28** (1989) 16.
[13] EGERTON R.F., *Ultramicroscopy* **4** (1979) 169.
[14] EGERTON R.F., Proc. 39th Ann. EMSA Meeting, Bailey G.W. Ed. (Claitor's Publishing, Baton Rouge, Lousiana, 1981) p. 198.
[15] HOFER F., *Ultramicroscopy* **21** (1987) 63.
[16] HOFER F., *Microsc. Microanal. Microstruct.* **2** (1991) 215.
[17] KRIVANEK O.L., SWANN P.R., in: Quantitative Microanalysis with High Spatial Resolution (The Metals Society, London, 1981) p. 136.
[18] EGERTON R.F., WILLIAMS B.G., SPARROW T.G., *Proc. Roy. Soc. Lond.* **A398** (1985) 395.
[19] EGERTON R.F., WANG Z.L., *Ultramicroscopy* **32** (1990) 137.
[20] LUO B., ZEITLER E., unpublished results.

[21] SHUMAN H., SOMLYO A.P., *Ultramicroscopy* **21** (1987) 23.
[22] LEAPMAN R.D., SWYT C.R. *Ultramicroscopy* **26** (1988) 393.
[23] MANOUBI T., TENCE M., WALLS M.G., COLLIEX C., *Microsc. Microanal. Microstruct.* **1** (1990) 23.
[24] PRESS W.H., FLANNERY B.P., TEUKOLSKY S.A., VETTERLING W.T., "Numerical Recipes in Pascal-The Art of Scientific Computing" (Cambridge University Press, 1989).
[25] LEAPMAN R.D., HUNT J.A., *Microsc. Microanal. Microstruct.* **2** (1991) 231.
[26] BRYDSON R., *EMSA - Bull.* **21** 57.
[27] HOFER F., Habilitationsschrift, Graz University of Technology (Graz, 1988).
[28] HANSEN P.L., MCCOMB D., BRYDSON R.D., *Micron. Microsc. Acta* **23** (1992) 1695.
[29] MCCOMB D., HANSEN P.L., BRYDSON R.D., *Microsc. Microanal. Microstruct.* **2** (1991) 561.
[30] EGERTON R.F., *Ultramicroscopy* **3** (1978) 243.
[31] HOFER F., WILHELM P., *Ultramicroscopy* **49** (1993) 189.
[32] AHN C.C., KRIVANEK O.L., ASU/Gatan EELS Atlas, Center for Solid State Science (Arizona State University , Tempe, AZ 85281, U.S.A., 1983).
[33] WALTER F., POSTL W. and TAUCHER J., *Mitt. Abt. Miner. Landesmuseum Joanneum* **58** (1990) 37.
[34] WALTER F., *Eur. J. Mineral* **4** (1992) 1275.
[35] ISAACSON M., JOHNSON D., *Ultramicroscopy* **1** (1975) 33.
[36] JOY D.C., MAHER D.M., *Ultramicroscopy* **5** (1980) 333.
[37] LEAPMAN R.D., NEWBURY D.E., *Anal. Chem.* **65** (1993) 2409.
[38] EGERTON R.F., *Ultramicroscopy* **50** (1993) 13.